How well do climate models simulate regional atmospheric circulation over East Asia?

Can Zhao, Zhihong Jiang, Xiaojuan Sun, Wei Li, Laurent Li

How well do climate models simulate regional atmospheric circulation over East Asia?

Can Zhao [1, 2], Zhihong Jiang [2, 3] *, Xiaojuan Sun [1, 2], Wei Li [1, 2], Laurent Li [4]

[1] Joint International Research Laboratory of Climate and Environment Change, Nanjing University of Information Science and Technology, Nanjing, China.

[2] Collaborative Innovation Center on Forecast and Evaluation of Meteorological Disaster, Nanjing University of Information Science and Technology, Nanjing, China.

[3] Key Laboratory of Meteorological Disaster of Ministry of Education, Nanjing University of Information Science and Technology, Nanjing, China.

[4] Laboratoire de Météorologie Dynamique, CNRS, Sorbonne Université, Ecole Normale Supérieure, Ecole Polytechnique, Paris, France.

*****Corresponding author. Mailing address: School of Atmospheric Science, Nanjing University of Information Science and Technology, No.219 Ningliu Road, Nanjing, Jiangsu, China. Telephone: +86-025-58731135. E-mail: zhjiang@nuist.edu.cn

Abstract

This study presents a comprehensive and quantitative evaluation of the mean state of summer atmospheric circulation over East Asia. Attention is paid to the South Asian high (SAH), western North Pacific subtropical high (WNPSH) and Indian low (IL) at the upper, middle and lower troposphere, respectively. A total of 31 state-of-the-art climate models from phase 5 of the Coupled Model Intercomparison Project (CMIP5) are used as examples for the analysis. Most models can basically simulate the three closed-circulation systems (CCSs), although there is a certain inter-model spread and an underestimation of their intensity. In terms of geographic location, models demonstrated the best performance for SAH and the poorest performance for WNPSH. The latter shows a generally south-westward shift compared to the National Centers for Environmental Prediction (NCEP) reanalysis. Five atmospheric fields (zonal and meridional wind at 850 hPa, geopotential height at 500 and 100 hPa and sea level pressure) are inspected and generally well reproduced in models, with Taylor-S indices all larger than 0.84 for 90% of the models. The best performance is for the geopotential height of 500 hPa with an average Taylor-S index of 0.98. Models' skill in simulating the sea level pressure is the lowest. However, a significant positive correlation with models' resolution is observed. Almost all models underestimate the 100 hPa geopotential height over East Asia, mainly due to the common cold bias in the troposphere. As a whole, CCSM4, CNRM-CM5, CESM1-CAM5 and NorESM1-M are identified as high-skill models for simulating the East Asian atmospheric circulation. High-skill models also show better simulation of precipitations in East China, with a 21.3% decrease of dry biases in Southeast China. The physical explanation for this

linkage is also reported to reside in the central position of the WNPSH, which determines the quality of 850 hPa winds and water vapour transport in Southeast China.

Key words atmospheric circulation, closed-circulation systems, CMIP5 models, western North Pacific subtropical high, Indian low, South Asian high, monsoon precipitation

1 Introduction

Atmospheric general circulation, allowing energy and water vapour to be redistributed over the Earth, is the most important factor controlling climate variation at both the global and regional scales. It contains a certain number of closed-circulation systems (CCSs) that can be either permanent or temporary and can exert profound impacts on regional climate. Many studies in the literature use this concept to investigate regional climate variability (e.g., Rossby, 1939; Akiyama, 1975; Khon and Mokhov, 2006; Han and Wang, 2007; Gamble et al., 2008; Li et al., 2011; Hameed and Reimer, 2012; Wang et al., 2012; Seo et al., 2013; Sun et al., 2017).

For East China, past studies demonstrated three dominant CCSs in summer. They are the Indian low (IL), western North Pacific subtropical high (WNPSH) and South Asian high (SAH). They have significant impacts on the regional precipitation. For example, moisture from the tropical oceans is transported to East China through the southerly flow at the western periphery of the WNPSH. Rainfall occurs at the north-western margin of the WNPSH, where warm moisture and cold air from high latitudes converge (Meehl et al., 2005; Zhou and Yu, 2005; Han and Wang, 2007; Liu et al., 2014; Preethi et al., 2017). A stronger IL, accompanied

by stronger water vapour transport at low latitudes, leads to increased rainfall in North China (Zhang, 2001; Liu and Ding, 2008; Ren et al., 2011).

Global climate models (GCMs) are primary tools for climate predictions and future climate projections. Evaluating the performance of atmospheric circulation in GCMs can increase our confidence in future projection. Much research directly considered atmospheric fields when evaluating model performance for the Asian monsoon (e.g., Duan et al., 2013; Gong et al., 2014; Jiang and Tian, 2013; Jiang et al., 2015; 2016; Li et al., 2018; Song and Zhou, 2014a, 2014b; Sperber et al., 2013; Xu et al., 2017; Wei et al., 2014; Zhou et al., 2018a). However, they rarely paid attention to model performance in terms of CCSs and their consistency with the relevant atmospheric fields. For those studies focusing on the SAH and the WNPSH (Liu et al., 2014; Qu and Huang, 2014; He and Hu, 2015; Tian et al., 2016; Xue et al., 2016), there is a general lack of consideration of models' systematic cold biases, which lower the geopotential height. It is worth noting that some recent studies used eddy geopotential height to measure the WNPSH, which partially overcomes the issue of geopotential height rise under global warming (He et al., 2015; Huang and Li, 2015; Huang et al., 2015; Wu and Wang, 2015; He et al., 2018). However, all types of biases cannot be corrected for using the concept of eddy geopotential height.

Wang et al. (2007, 2010) proposed an alternative algorithm dealing with a CCS, which provides a unified definition of indices, including centre position and intensity, to suitably describe CCSs. The algorithm, together with a few adaptations and ameliorations, is described in next section.

The main objective of this study is twofold. First, we aimed to document CMIP5 model performance in simulating the mean state of atmospheric fields and main CCSs over East Asia and to study models consistency among different evaluated targets. Second, we wanted to investigate how biases in atmospheric circulation exert impacts on biases in precipitation.

This paper is organized as follows: Section 2 shows the data and methodology. Section 3 presents a comprehensive assessment and consistency comparison of the atmospheric fields and the major CCSs. Section 4 discusses the influence of simulated atmospheric fields and CCSs on the simulated precipitation in eastern China. Section 5 presents final conclusions for the whole work.

2 Data and Methods

2.1 Models, Simulations and Reference Data

Our study area covers a large zone in East Asia, 10–70°N, 60–160°E. The regional mean state of atmospheric circulation is evaluated for 45 years, from 1961 to 2005. Variables from 31 CMIP5 models are used in this study, including monthly geopotential height at 100 hPa (Z100) and 500 hPa (Z500), zonal (U850) and meridional (V850) wind at 850 hPa, sea level pressure (SLP), atmospheric temperature and daily precipitation accumulation. Only one historical run is chosen for each model (r1i1p1) to ensure that the evaluation is unbiased. Table 1 shows the relevant basic information of these CMIP5 models. To facilitate the comparison, a bilinear interpolation scheme was used to transform variables from their native grids to a 2.5 × 2.5° common grid. The three CCSs evaluated in this study are listed in Table 2.

103 **Table 1** Acronyms, resolutions and institutions of the 31 CMIP5 Models. The first
104 column shows models serial number in this paper, listed in alphabetic order. Expansions of
105 model acronyms are available at http://www.ametsoc.org/PubsAcronymList

No.	Models name	LON. × LAT.	Modeling center or group
1	ACCESS1.0	1.875°×1.25°	Commonwealth Scientific and Industrial Research Organization and Bureau of Meteorology
2	ACCESS1.3	1.875°×1.25°	
3	BCC-CSM1.1	～2.8125°×2.8125°	Beijing Climate Center, China Meteorological Administration
4	BCC-CSM1.1(m)	～1.125°×1.125°	
5	BNU-ESM	～2.8°×2.8°	Beijing Normal University
6	CanESM2	～2.8125°×2.8125°	Canada Center for Climate Modeling and Analysis
7	CCSM4	0.9°×1.25°	US National Centre for Atmospheric Research
8	CESM1-CAM5	0.9°×1.25°	Commonwealth Scientific and Industrial Research Organization and Bureau of Meteorology
9	CMCC-CM	0.75°×0.75°	Centro Euro-Mediterraneo per I Cambiamenti Climatici
10	CMCC-CMS	1.875°×1.875°	
11	CNRM-CM5	～1.4°×1.4°	Centre National de Recherches Meteorologiques-CERFACS
12	EC-EARTH	～1.125°×1.125°	EC-EARTH consortium
13	FGOALS-g2	2.8125°×2.8125°	Institute of Atmospheric Physics, Tsinghua University
14	FGOALS-s2	2.81°×1.66°	Institute of Atmospheric Physics, Chinese Academy of Sciences
15	GFDL-CM3	～2.5°×2.0°	NOAA Geophysical Fluid Dynamics Laboratory
16	GFDL-ESM2G	～2.5°×2.0°	
17	GFDL-ESM2M	～2.5°×2.0°	
18	HadCM3	3.75°×2.5°	Met Office Hadley Centre
19	HadGEM2-CC	1.875°×1.25°	
20	HadGEM2-ES	1.875°×1.25°	
21	IPSL-CM5A-MR	1.25°×2.5°	Institut Pierre Simon Laplace
22	IPSL-CM5A-LR	1.5°×3.75°	
23	MIROC4h	0.5625°×0.5625°	University of Tokyo, National Institute for Environmental Studies Japan Agency for Marine - Earth Science and Technology
24	MIROC5	1.40625°×1.40625°	
25	MIROC-ESM	2.8125°×2.8125°	
26	MIROC-ESM-CHEM	2.8125°×2.8125°	
27	MPI-ESM-LR	～1.8°×1.8°	Max Plank Institute for Meteorology
28	MPI-ESM-MR	～1.8°×1.8°	
29	MPI-ESM-P	～1.8°×1.8°	
30	MRI-CGCM3	1.125°×1.125°	Meteorological Research Institute
31	NorESM1-M	2.5°×1.9°	Norwegian Climate Centre

Table 2 Closed-circulation systems and their corresponding original fields from which they are deduced.

Acronyms	Closed-circulation systems	Original fields
IL	India Low	sea level pressure
WNPSH	western North Pacific subtropical high	500hPa geopotential height
SAH	South Asian High	100hPa geopotential height

In terms of observations used as a reference, we use reanalysis data from the National Centers for Environmental Prediction - National Center for Atmospheric Research (NCEP/NCAR), with a resolution of 2.5 × 2.5°. For precipitation, a high - quality gridded dataset deduced from surface stations in China with a resolution of 0.5 × 0.5° is used as the reference (Chen et al., 2010).

2.2 Model Performance Metrics

2.2.1 Taylor Diagram

Taylor Diagram (Taylor, 2001) is designed to assess the matching degree of spatial pattern between models and the reference. It is a diagram summarizing the centered (spatial mean removed) root-mean square error (RMSE), correlation coefficient R and ratio σ_f of standard deviations (RSD) between models and the reference. Two of the three parameters are independent and the third one can be deduced. Taylor-S index (Taylor, 2001) uses the two independent parameters to form a combined indicator useful for quantitative evaluation:

$$S = \frac{4(1+R)}{\left(\sigma_f + 1/\sigma_f\right)^2 \left(1+R_0\right)} \quad (1)$$

where R_0 is the maximum correlation attainable (R_0 = 1 in this study).

2.2.2 Indices for describing closed-circulation systems

A complete set of Closed-Circulation-System Indices (CCSI) proposed by Wang et al. (2007, 2010) is used to quantitatively describe closed-circulation systems, including center position (λ_c, θ_c) and intensity P. In previous studies using CCSI, the critical isobar (the largest closed iso-line) f_0 in the calculation of CCSI was generally determined by a predefined climatological value (e.g. Ren et al., 2011; Sun et al., 2013, 2017; Wang et al., 2012). In order to reduce the bias of f_0 selection, the most outside closed iso-line of the closed-circulation system is defined as the critical isobar f_0 in this study. Ω is the domain where the main body of the closed circulation system locates. Computational domain D is the common area of Ω and f_0. Take the western North Pacific subtropical high from NCEP data as an example, the geopotential height at 500hPa is shown in Fig. 1. Ω is the blue box domain (110-180° E，0-40°N), critical isobar f_0 is the outer edge of the cyclone circulation (5860gpm shown here as bold black contour), and D is the shaded domain. For the South Asian high and the Indian low, the search domains Ω are (110-180°E, 10-50°N) and (30-100°E, 10-40°N) respectively.

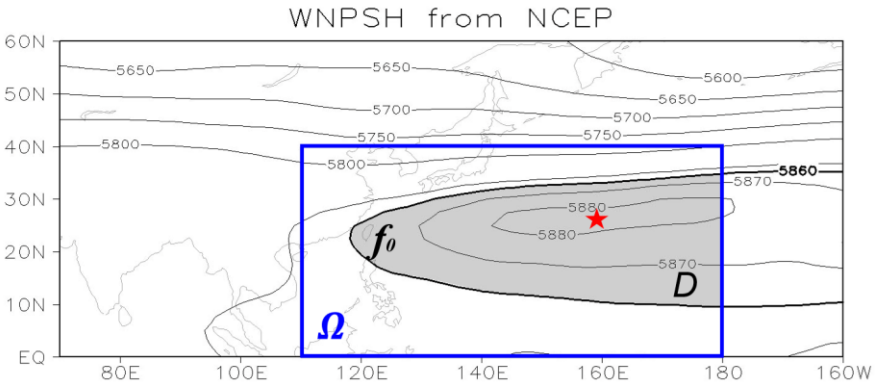

Figure 1. WNPSH from NCEP represented by climatological geopotential height at 500hPa as example to show the critical isobar f_0, search domain Ω, and computational domain D

By denoting **r** as the positions vector for the grid (λ,θ) on the Earth sphere, $f(\mathbf{r})$ represents the geopotential height at gird (λ,θ), and f_0 represents the value of critical isobar. The intensity index *P* is the area integral of the values of geopotential height difference fields ($df = f(\mathbf{r}) - f_0$) in domain D. The center position index (λ_c ,θ_c) is the barycenter of the difference fields *df*. The position vector for (λ_c ,θ_c) is represented by $\mathbf{r_c}$. *P* andλ_c, θ_c can be calculated from the following equation:

$$P = \left[\iint_D f(\lambda,\theta) - f_0 \right] ds \tag{2}$$

$$\iint_D \left| f(\mathbf{r}) - f_0 \right| (\mathbf{r} - \mathbf{r}_c)\, ds = 0 \tag{3}$$

The value of P is positive for high-pressure center, and negative for low-pressure center. For the high-pressure center, larger the value of P, stronger the closed-circulation system is, the low-pressure center converses. We define the radius of the earth as a unit radius, so unit of *P* is Pa•rad^2 for the Indian Low and gpm•rad^2 for the South Asian high and western North Pacific subtropical high. A square of 1 rad^2 corresponds to Earth surface area of 40.6 million km^2 at equator, and decreases with cosine of the latitude.

For the evaluated models, Ω is the same as in NCEP for each circulation system, but the critical isobar f_0 varies from one model to another. f_0 of each model shows its systematical bias. It can be considered as a comprehensive parameter of each individual model. By using the last closed iso-line of a closed-circulation system as its critical isobar,

we can easily deduce that the intensity parameter actually reveals the spatial gradient of the closed-circulation system, an important measure for any geophysical flow. It is clear that the proposed CCS indices can objectively represent the properties of any closed-circulation systems in climate models.

2.2.3 Comprehensive Ranking Measure M_R

To assess model's performance and consistency among multiple properties and indices, the comprehensive ranking measure M_R as defined in Radić and Clarke (2011) is used in this study:

$$M_R = 1 - \frac{1}{(n \times m)} \sum_{i=1}^{m} rank_i \quad (4)$$

where m is the number of indices entering into the calculation, n is the number of evaluated models. $rank_i$ is the model performance rank for the index i. The closer the value of M_R to 1, the better the model comprehensive performance is (Chen et al., 2011; Jiang et al., 2012, 2015; You et al., 2018).

3 Models Performance in the Mean State of Atmospheric Circulation

This section gives firstly models performance in simulating the mean state of five atmospheric fields with the Taylor-S index. It pursues by a presentation of models performance in simulating the mean state of three closed-circulation systems with CCS indices. Finally, models consistency and comprehensive capabilities are evaluated with M_R index.

3.1 Evaluation of Atmospheric Fields

Figure 2 displays the Taylor diagram showing the performance of models in simulating five atmospheric fields with NCEP data as reference. The number next to each point corresponds to models order listed in Table 1. We can see that the five atmospheric fields are well reproduced, with correlation coefficients all larger than 0.6. Models have the best skill in simulating the geopotential height, especially the 500hPa geopotential height (Z500), for which models also show the smallest inter-model spread. Such a result is in agreement with previous studies (e.g. Belleflamme et al., 2013; Gong et al., 2014; Tian et al., 2016).

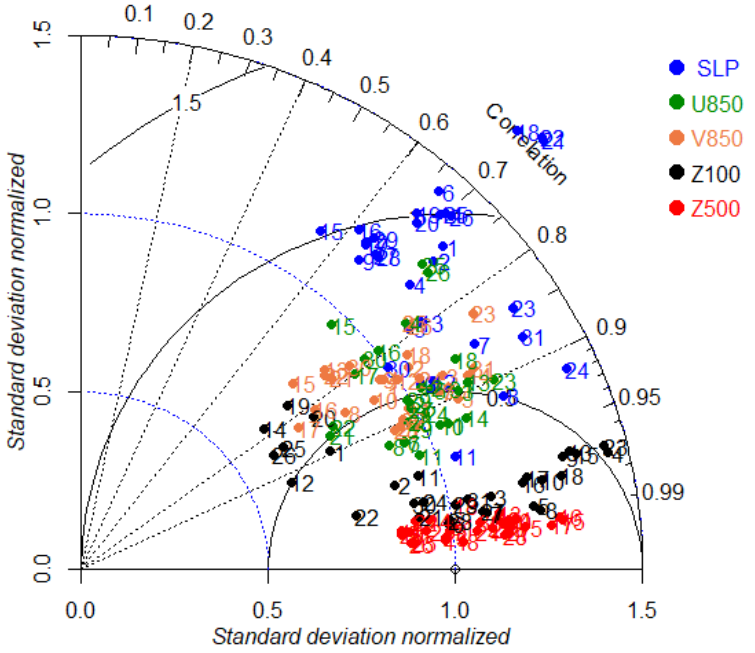

Figure 2. Taylor diagram obtained from five atmospheric fields, Sea Level Pressure (SLP), zonal (U850) and meridional wind (V850) at 850hPa, and geopotential height at 100hPa (Z100) and 500hPa (Z500), and from 31 CMIP5 models. Radial lines emanating from the origin (0.0, 0.0) display the spatial correlation coefficients between simulations and the reference NCEP, radial circles show

191 models standard deviations normalized by their counterpart from NCEP, and solid circles indicate the
192 root-mean square difference between models and NCEP field. The number next to each point
193 corresponds to the model number listed in Table 1.

194 The Taylor-S index for Z500 varies from 0.93 to 0.998, with the average value of 0.98.
195 For 100hPa geopotential height (Z100), the Taylor-S index ranges from 0.72 to 0.995 with
196 average value of 0.92. Most models have their spatial correlation coefficients with NCEP
197 larger than 0.9. However, there is a large inter-model spread for the spatial variance, with the
198 normalized standard deviations from 0.4 to 1.51. In addition, all models, except
199 CanESM2(6#), have negative bias (lower height) for Z100 compared with NCEP. The
200 underestimation of Z100 is not a local manifestation in East Asia, but occurs over the globe.
201 The vertically averaged temperature (VAT) between the surface and isobaric surface p = 100
202 hPa are calculated for NCEP data and CMIP5 models outputs. Results show that all models
203 have a globally-averaged cold bias. The inter-model correlation between the bias of VAT
204 and the bias of 100hPa geopotential height is 0.55, as shown in FIG. 3.

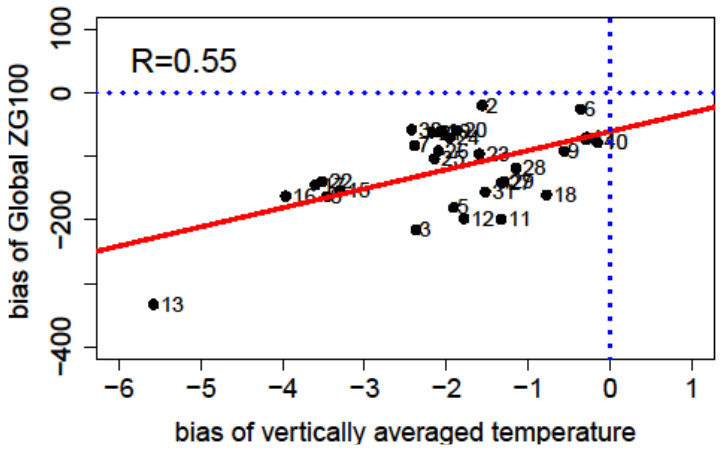

205

Figure 3. Scatter diagram showing the globally-averaged biases of tropospheric temperature (abscissa-axis) and the globally-averaged biases of 100hPa geopotential height (ordinate-axis) from the 31 models. R is the inter-model correlation coefficient between the two biases. The red solid line is the linear regression.

Models have the lowest skill in simulating sea level pressure (SLP), with average Taylor-S index of 0.79. There is a large inter-model spread and the correlation coefficients with NCEP vary from 0.6 to 0.95. Models performance in simulating SLP seems largely in connection with models resolution. The inter-model rank correlation coefficient between the Taylor-S index for SLP and models resolution is as high as 0.6. Another feature revealed by the Taylor diagram is that all models overestimate the spatial variance of SLP, since the normalized standard deviations (radial circles) against NCEP data are all above 1.0. Models can reasonably reproduce 850hPa zonal and meridional wind. Correlation coefficients with NCEP vary from 0.75 to 0.95. Models have a similar performance in zonal and meridional winds, their Taylor-S indices being of 0.89 and 0.88 respectively.

Table 3 Spearman rank correlation coefficients for each pair of two rankings among the five atmospheric fields (SLP, U850, V850, ZG500 and ZG100) and the three closed-circulation systems. Bold figures show the statistical significance at $\alpha = 0.05$ level ($t_{\alpha,31} = 0.344$). The ranking for the atmospheric fields was based on their Taylor-S values, and the ranking for the closed-circulation systems was based on their absolute biases evaluated through the close-circulation-system indices.

	SLP	**U850**	**V850**	**ZG500**	**ZG100**	**WNPSH**	**SAH**

U850	**0.37**						
V850	**0.43**	**0.73**					
ZG500	0.24	**0.38**	**0.35**				
ZG100	0.27	0.31	**0.43**	0.26			
WNPSH	0.28	0.11	0.27	0.07	0.31		
SAH	0.27	0.26	**0.43**	0.34	**0.53**	**0.44**	
IL	**0.44**	0.01	0.13	0.27	0.09	0.08	0.24

To evaluate models consistency among the five atmospheric fields, inter-model rank correlation is calculated and shown in Table 3. Models rank was determined with the Taylor-S index, higher Taylor-S index corresponding to higher rank. We can see that models have the best consistency between zonal wind and meridional wind, with the rank correlation coefficient reaching 0.73. Moreover, models rank for 850hPa meridional wind has a good correlation with the rank from other fields. Although models rank can be divergent among different atmospheric fields, the high-skill models, such as CCSM4 (7#) and CNRM-CM5 (11#), have an excellent behavior for almost all variables.

3.2 Evaluation of closed-circulation systems

Center location and intensity of the South Asian high (SAH), Indian low (IL) and western North Pacific subtropical high (WNPSH) simulated by CMIP5 models and from NCEP data can be assessed with the closed-circulation-system indices which allow the removal of models systematic but less-or-not-relevant biases such as too-low geopotential height in models. Results are shown in FIG. 4.

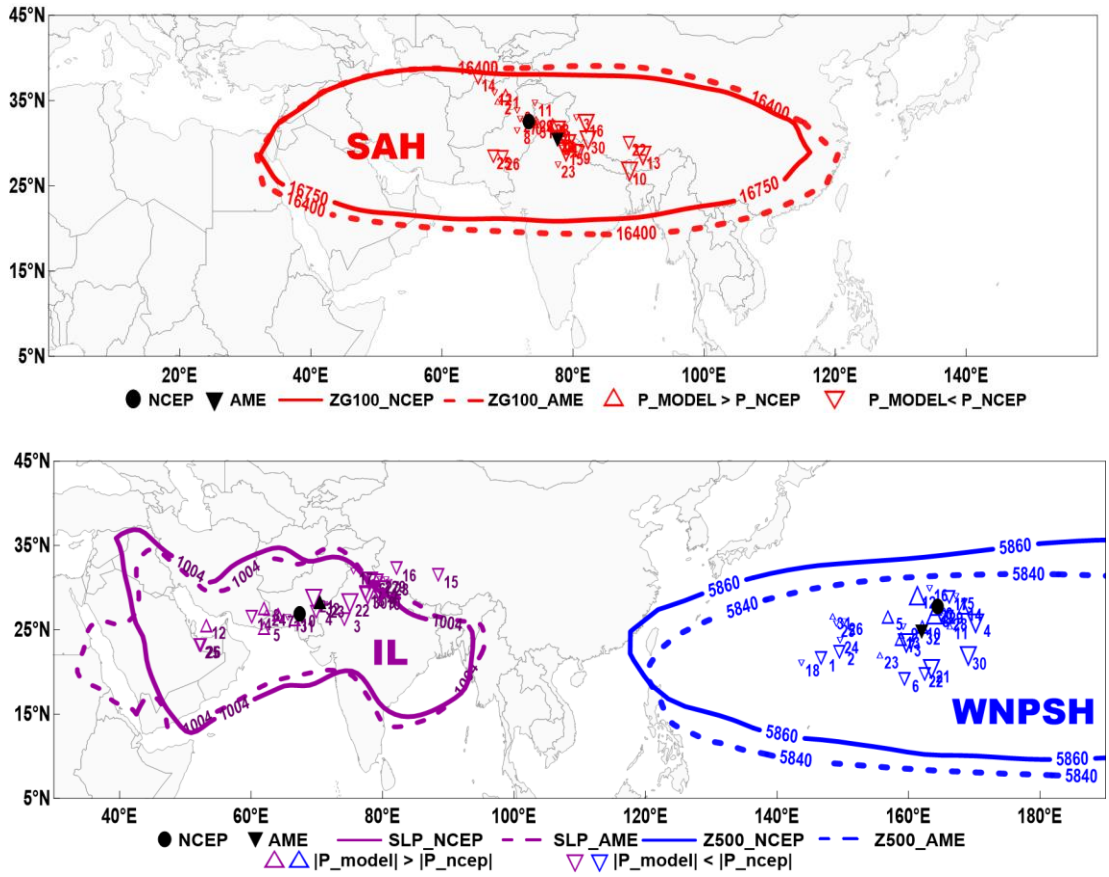

Figure 4. The three closed-circulation systems represented in the upper panel for the South Asian high (SAH) and in the lower panel for the Indian low (IL) and western North Pacific subtropical high (WNPSH). Solid contours show their limitation boundaries as depicted in NCEP reanalysis: the line 16750 gpm at 100 hPa for SAH, the line 1004 hPa at sea level for IL, and 5860 gpm at 500 hPa for WNPSH. Dashed contours are the counterpart from models as an ensemble mean. Center position and intensity for each CMIP5 individual model are plotted for the three closed-circulation systems respectively. Position is marked by either triangles or inverted triangles. Intensity is shown with the size and form of the symbols: an inverted triangle if | P_model | < | P_ncep | and a triangle if | P_model | > | P_ncep |. The size of the symbols represents amplitude of the deviation. The position of the multi-model ensemble is marked by a solid and black inverted triangle, and the position of NCEP by a solid black circle.

253 It can be seen that, although there is a large inter-model spread for the simulated center
254 location, all models have the basic capability of simulating the three closed-circulation
255 systems. Models have the best performance and the smallest inter-model spread in simulating
256 the location of SAH, the average value and standard deviation of distances between models
257 and NCEP being 599 km and 418 km respectively (Table 4). Most models simulate a
258 southeast-shifted center of SAH compared with NCEP (FIG.4). The inter-model correlation
259 coefficient between simulated bias in center latitude and longitude of SAH is -0.6. 71% of
260 models underestimate the intensity of SAH. The inter-model rank correlation coefficient
261 between the center position and intensity of SAH is 0.67. It indicates that, for SAH, models
262 with high skill in simulating the center location usually have good performance for intensity.

263 **Table 4** Average distance of simulated closed-circulation system from their counterpart
264 in NCEP, together with the standard deviation among models. Unites: km.

	Indian Low	**South Asian high**	**western North Pacific subtropical high**
Average distance	952	599	805
Standard deviation	505	418	586

265 There is a large inter-model spread for the location of IL. Two-thirds of the models
266 simulate a northeast-ward shift compared with NCEP. Inter-model correlation coefficient
267 between biases in center latitude and those in longitude is 0.89, which explains why models
268 tend to be on a diagonal line from southwest to northeast. It is also interesting to note that
269 those models situated in the northeast side of NCEP in Fig. 4b all underestimate the intensity.
270 The largest inter-model spread for center position is from WNPSH (Table 4). Most models
271 have a southwest-shifted center. Only 4 models simulate a north-shifted center of WNPSH

compared with NCEP. Nearly half of the models simulate a stronger WNPSH, but most of the positive deviations are small.

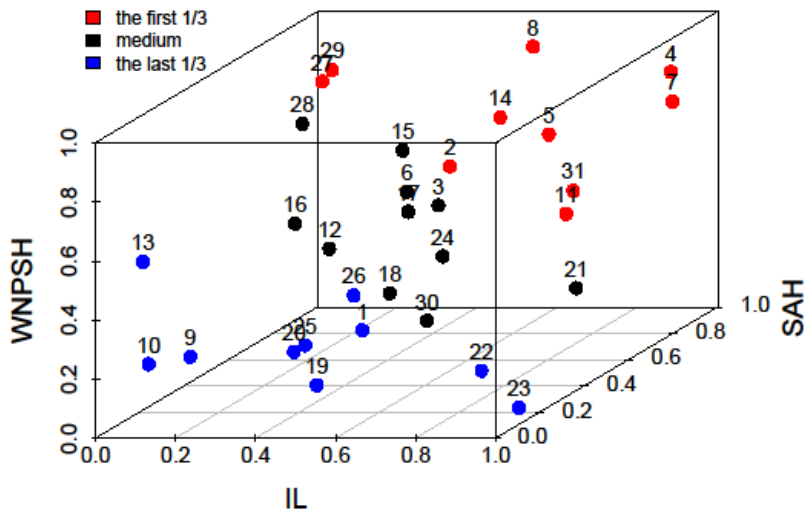

Figure 5. Three-dimensional scatterplot for the three comprehensive indices M_R from ranking performed on the three closed-circulation systems, Indian low (IL), South Asian high (SAH) and western North Pacific subtropical high (WNPSH) respectively. Numbers over each point are consistent with models serial number shown in Table 1. Following their comprehensive performance ranking, models in the top third are plotted in red color, while those in the bottom third are in blue.

Figure 5 shows the scatterplot of comprehensive indices M_R for the Indian low (IL), South Asian high (SAH) and western North Pacific subtropical high (WNPSH). The performance of models is quite divergent among the three closed-circulation systems. The rank correlation coefficient between WNPSH and IL is only 0.08 (Table 3) indicating almost no correlation at all. It is to be noted that, despite divergent performance for CMIP5 models in simulating the three closed circulation systems, top ranked models and bottom ranked models have good consistency respectively. For example, BCC-CSM1.1 (m) (4#) and

CCSM4 (7#) have an excellent performance for all the three closed circulation systems. CMCC-CM (9#) and CMCC-CMS (10#) have the poorest performance for the circulation systems.

3.3 Comprehensive Performance and Consistency

To evaluate models consistency among different variables, Figure 6 shows models rank for each evaluated variable by color blocks. For atmospheric fields, models are ranked by their Taylor-S index, with high value corresponding to good rank. For closed-circulation systems, models are ranked according to their absolute biases of the relevant indices. In Fig. 6, models rank is consistently indicated with colors as in the color bar. From top to bottom, models comprehensive performance determined by multiple M_R goes from the best to the worst. It can be seen that the rank of a model depends on the selection of assessment variables. This result seems in agreement with a few previous studies (Gleckler et al., 2008; Jiang et al., 2016; Ou et al., 2013; Radić et al., 2011; Sheffield et al., 2013a, 2013b; Su et al., 2013; Xu et al., 2017). We can note, however, that top ranked models and bottom ranked models have good consistency. Bad consistency is mainly manifested in the models at middle levels of the ranking. Results shown in Fig. 6 can serve as guidance for selecting global models outputs for regional climate downscaling, and can provide useful information for climate projection within a framework of multi-model ensemble, models ranking being useful in assigning weight for each model.

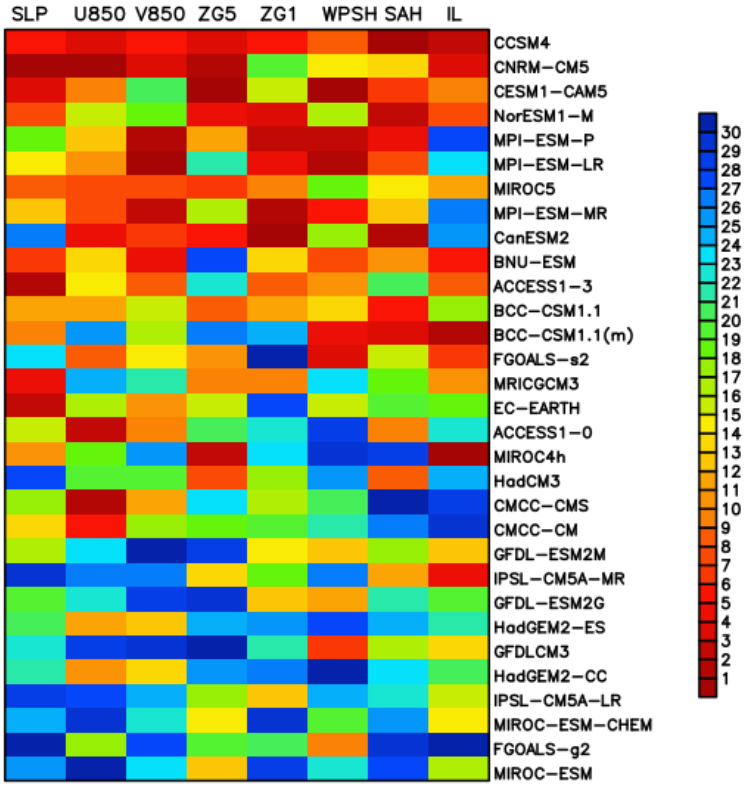

306

307 **Figure 6**. Portrait diagram with color blocks showing models ranking (as indicated by the color label
308 bar) performed separately on the five atmospheric fields: sea level pressure (SLP), zonal (U850) and
309 meridional (V850) wind at 850hPa, and geopotential height at 500hPa (ZG5) and 100hPa (ZG1); and
310 on the three closed-circulation systems: western North Pacific subtropical high (WNPSH), South
311 Asian high (SAH) and Indian low (IL). Models acronyms listed on the right follow their total record
312 of ranking. From top to bottom, models go with decreasing performance.

313 Inter-model correlation between each pair of two rankings are calculated and shown in
314 Table 3 which allows us to examine the consistency between closed-circulation systems and
315 their original atmospheric fields from which they are deduced (listed in Table 2). The South
316 Asian high has the best consistency with 100hPa geopotential height, the rank correlation
317 coefficient being 0.53. The Indian low shows a rank correlation coefficient of 0.44 with the

318 sea level pressure. Finally, the western North Pacific subtropical high has the poorest
319 correlation with 500hPa geopotential height, the rank correlation being only 0.07.

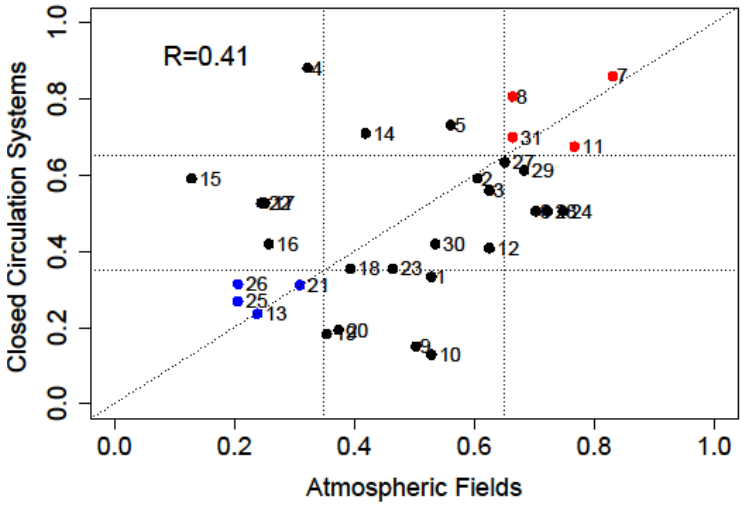

320

321 **Figure 7**. Scatter diagram for models comprehensive index from atmospheric fields (x axis: including
322 sea level pressure, geopotential height at 100hPa and 500hPa, zonal wind and meridional wind at
323 850hPa) and that from closed-circulation systems (y axis: Indian low, South Asian high and western
324 North Pacific subtropical high). Number next to each point is consistent with models serial number
325 shown in Table 1. R is the correlation coefficient between the two measures in X axis and Y axis.

326 Let us now examine how the comprehensive index M_R from the closed-circulation
327 systems is consistent with that from the corresponding atmospheric fields. The scatter
328 diagram in Fig. 7 displays each model as a point with its ordering number, the x-axis being
329 the comprehensive index M_R from all atmospheric fields, and the y-axis being that from all
330 closed-circulation systems. Models situated in the upper right corner have the best
331 performance in the two indices from both the closed-circulation systems and their
332 corresponding atmospheric fields, while converse in the bottom left corner. There would be
333 a perfect consistency between the models performance in simulating the two properties if all

dots in Fig. 7 were on the diagonal. The actual inter-model correlation coefficient between the two is 0.41. It would be significantly increased (value =0.62) if models BCCCSM1.1(m) (4#), CMCC-CMS (10#) and GFDL-CM3 (15#) (at the periphery of the collection of points) were kicked off from the ensemble. Figure 7 can also allow us to select high-skill models (red dots) and low-skill ones (blue dots) in a highly-synthetic way with consideration of M_R from both atmospheric fields and closed-circulation systems. Red dots in Fig. 7 have M_R values larger than 0.65. They are from CCSM4, CNRM-CM5, CESM1-CAM5 and NorESM1-M respectively. They can be qualified as high-skill models within our evaluation.

4 Influence of atmospheric circulation on precipitation at inter-model level

In observation as well as in numerical models, East Asian monsoon precipitation is closely related to atmospheric circulation in the region (He and Zhou, 2014; Song and Zhou, 2014; Zeng et al., 2012; Zhou et al., 2018b). For example, there is a significant correlation between the low-level meridional wind jet and precipitation over East China. The western North Pacific subtropical high largely determines the East Asian summer monsoon rainfall band (He and Zhou, 2014; Song and Zhou, 2014). In this section, we want to check if similar relations exist between rainfalls in East Asia and regional atmospheric circulation within the framework of inter-model variability. In other words, we want to check if good models for circulation are also good for rainfalls. Since monsoon precipitation is dependent on many circulation factors, it is thus preferable to choose models following their comprehensive performance. High-skill models and low-skill models, as selected in the previous section, can be used to explore the impacts of atmospheric circulation biases on precipitation biases. As shown earlier, four models (CCSM4, CNRM-CM5, CESM1-CAM5 and NorESM1-M) are

selected for the high-skill models ensemble (HME), and FGOALS-g2, MIROC-ESM, MIROC-ESM-CHEM and IPSL-CM5A-LR are included in the low-skill models ensemble (LME).

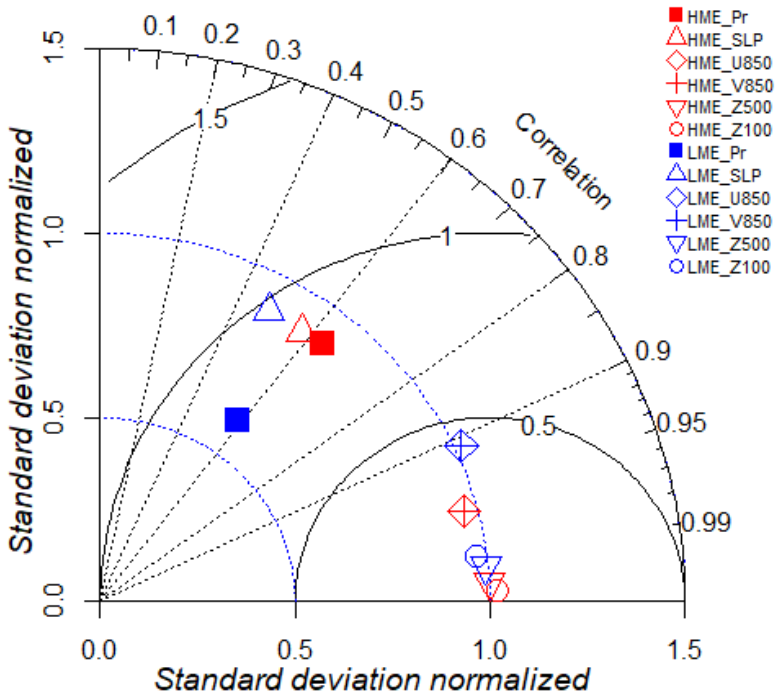

Figure 8. Taylor diagram for the five atmospheric fields (AFs) over East Asia and the precipitation distribution in East China. The assessment was done for the high-skill models ensemble (HME, in red) and the low-skill models ensemble (LME, in blue) respectively. The reference for atmospheric fields was from NCEP, and that for precipitation from surface observation.

Figure 8 displays the Taylor diagram showing precipitation (solid symbols) in East China and atmospheric circulation fields (hollow symbols) over East Asia in HME (in red) and LME (in blue) respectively. For precipitation in East China, it is easy to see that HME remarkably reduces the deviation compared to LME, which obviously underestimates the spatial variability of precipitation. The standard deviation in HME is much closer to observation than in LME, their normalized standard deviations being 0.9 and 0.6 respectively.

In terms of geographic distribution of precipitations in East China, we perform an inter-model empirical orthogonal function (EOF) analysis on the precipitation biases of 31 models in East China, to analyze the dominant modes of inter-model variations in the average precipitation bias. Figure 9 shows the first inter-model EOF mode which accounts for most (53.5%) of the total inter-model variance. It is characterized by the "wet-north and dry-south" structure of precipitation biases for the most models. Such a result that dry biases in Southeast China and wet biases in Northeast China is in agreement with previous studies (Chen et al., 2014; Ou et al., 2013; Jiang et al., 2015). For PC1, all models from HME and LME have positive value. Such a situation is visible for both HME and LME as well, shown in Figure 10. The dry biases in the south are smaller in HME than in LME by about 21.3%.

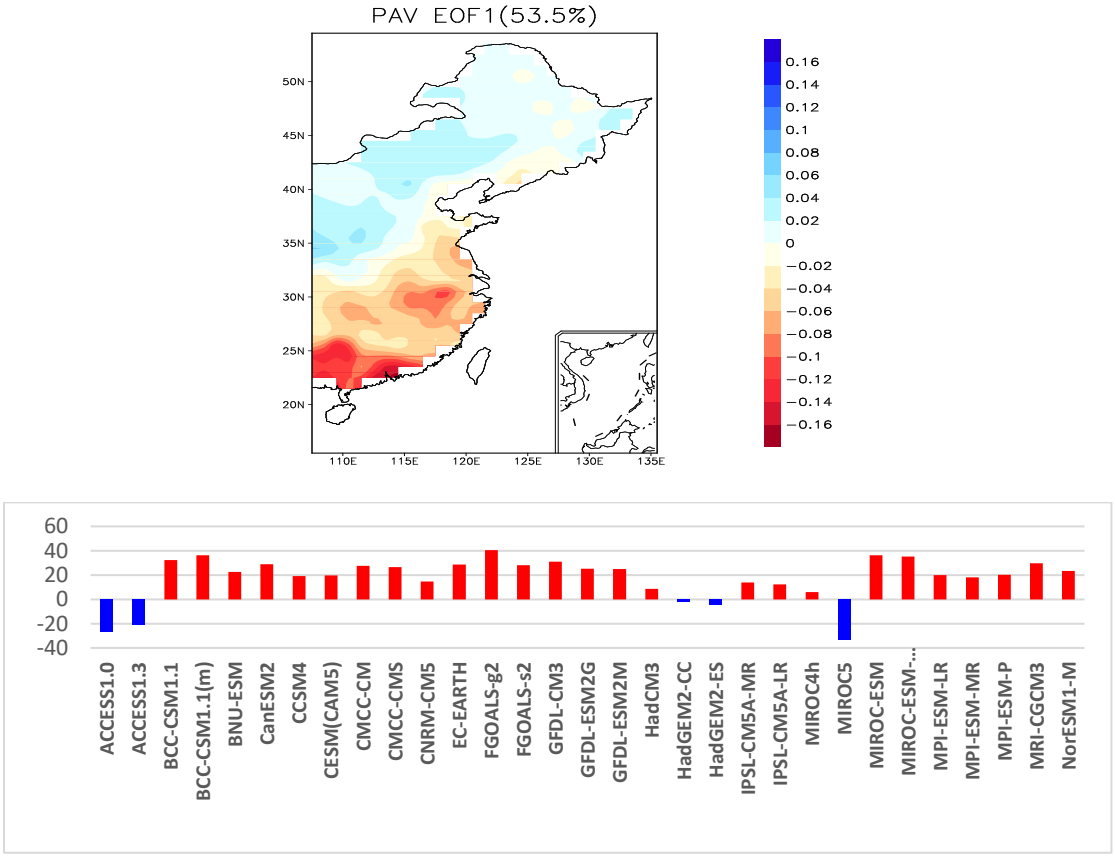

382 **Figure 9.** Upper panel shows the first EOF mode of the climatology precipitation bias in East China
383 calculated by inter-model EOF from 31 models. Lower panel shows the corresponding PC, with red
384 for positive value and blue for negative value.
385

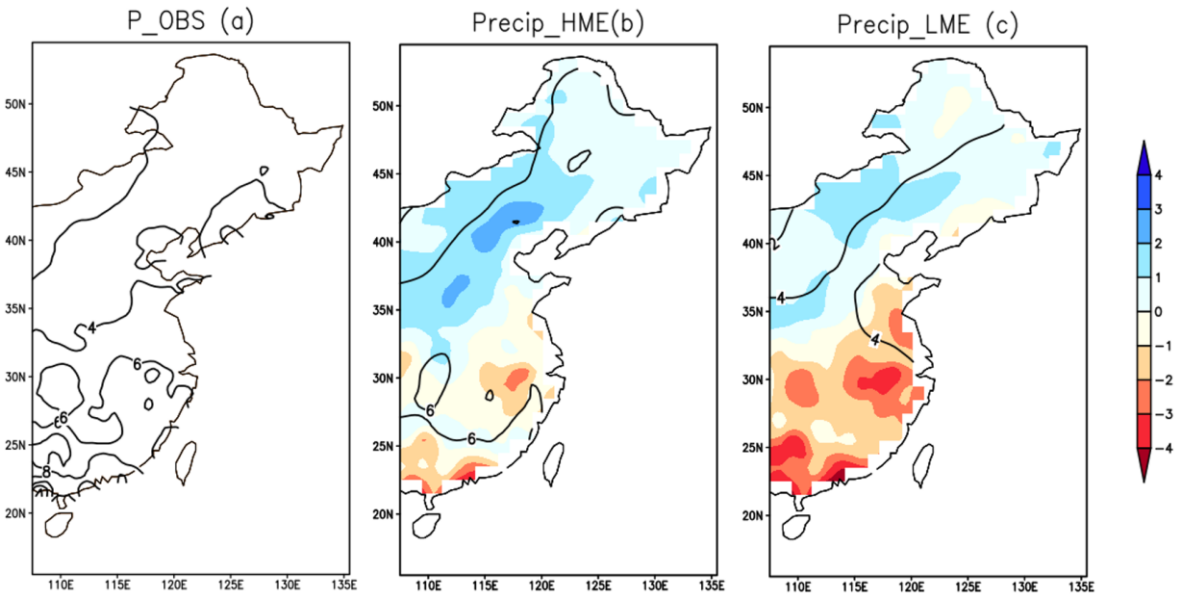

386

387 **Figure 10**. Distribution maps of average precipitation in summer in East China (contours, mm/day)
388 from (a) observation, (b) high-skill models ensemble (HME) and (c) low-skill models ensemble
389 (LME). Deviations from the observation are shown in shaded for HME and LME.

390 After exploring behaviors of the regional precipitation, we pursue our analyses on
391 atmospheric fields and closed-circulation systems which can behave differently in HME and
392 LME. Figure 8 shows clearly that there is a better performance for atmospheric fields in HME
393 than in LME. The most obvious improvement is for 850hPa zonal and meridional wind
394 (crosses and rhombuses). HME also has a better performance for all the three closed-
395 circulation systems. In particular, it shows prominent advantages for intensity of the Indian
396 low and position of the western North Pacific subtropical high (Table 5). Compared to NCEP,

LME shows a westward shift about 9 degrees in longitude for the center of the western North Pacific subtropical high. LME also has a weaker Indian low, as the difference of intensity with NCEP is 31.21 Pa•rad^2 (for low-pressure system, the intensity index is smaller than zero). For the South Asian high, LME has only a little decrease of performance compared to HME.

Table 5

Center Coordinates, Intensity (P) and critical isobar (f_0) of the Indian low (IL), South Asian high (SAH) and western North Pacific subtropical high (WNPSH) from NCEP, and deviations from NCEP in HME and LME. Latitude is positive northward and longitude is positive eastward. Unites of P: Pa•rad^2 for IL, gpm•rad^2 for SAH and WNPSH.

	IL			**SAH**			**WNPSH**		
	center	**P**	f_0	**center**	**P**	f_0	**center**	**P**	f_0
NCEP	(66.1, 26.1)	-54.3	1004	(73.3,33.3)	15.3	16750	(164.5, 27.8)	4.1	5860
HME-NCEP	(-1.9, -0.3)	-5.2	0	(-0.1, -0.8)	-0.8	-150	(0.2, -1.8)	-1.1	0
LME-NCEP	(-6.7, -2.4)	31.21	4	(-2.3, -1.8)	-0.8	-1400	(-8.7, -1.8)	-3.6	-10

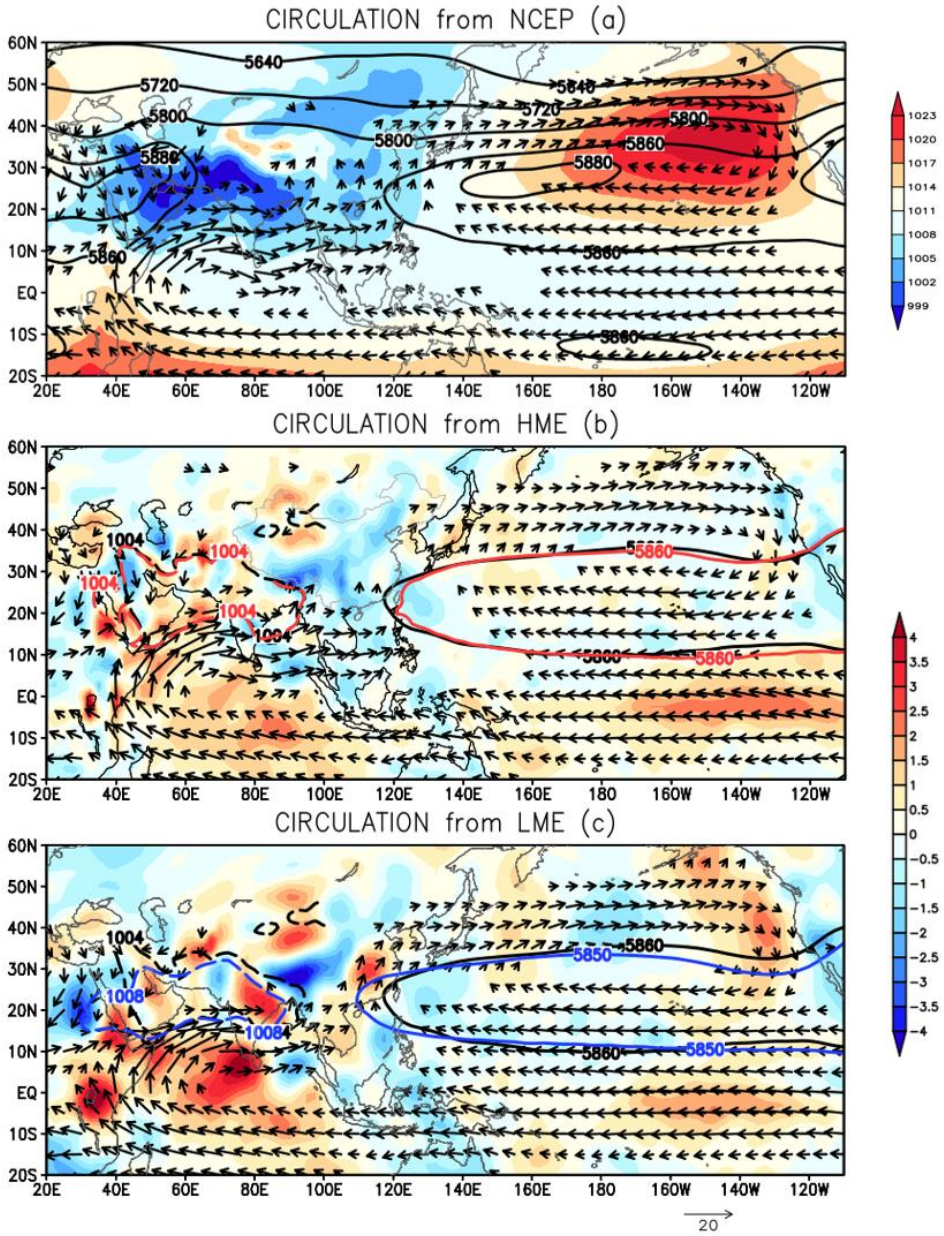

406

407 **Figure 11**. Upper panel (a) shows 850hPa wind vectors (ms^{-1}), 500hPa geopotential height (contours)
408 and sea level pressure (shading) as depicted in NCEP reanalysis. Middle panel (b) shows 850hPa
409 wind vectors (ms^{-1}), the critical lines f_0 to delimit the outside edge of the western North Pacific
410 subtropical high (solid line in red) and the Indian low (dotted line in red) as depicted in HME (critical
411 lines of NCEP reanalysis are also marked in black contours). Shading represents 850hPa meridional

412 wind deviation from NCEP (ms^{-1}). Lower panel (c) is the same as (b), but for LME (critical lines are
413 in blue instead of red). 850hPa wind vectors are omitted when smaller than 3 m/s in the three panels.

414 From the above analyses, we can see that HME, with an improvement of the
415 atmospheric circulation, does improve precipitations in East China. Similarly, LME with a
416 deterioration of the atmospheric circulation shows bad performance for the regional
417 precipitation. We want now to confirm this conclusion through compositing all models for
418 HME and LME. We also want to investigate the relevant physics behind this relationship, in
419 particular, how water vapor transport can influence wetness or dryness in the region. Figure
420 11(a) shows 850hPa wind fields representing the low-level water vapor paths over and
421 surrounding East Asia from NCEP data. It can be seen that, the main components of the water
422 vapor paths for East China include the southwesterly flows along the east coast of the Arabian
423 Peninsula, the southwesterly flows and westerlies extending from the Arabian Sea to the
424 Philippines, the southerlies from the South China Sea, and the southeasterly flows along west
425 flank of the Western North Pacific Subtropical High. Previous studies show that this water
426 vapor path from the Arabian Sea to East China exerts an important influence on the
427 precipitation in East China (Jiang et al., 2015; Simmonds et al., 1999; Tao and Chen, 1987;
428 Xu et al., 2008).

429 HME depicts well these water vapor paths. The southwesterly flows in East China are
430 well reproduced, especially for the meridional wind fields in Southeast China (shaded in FIG
431 11b), which are very close to what depicted in NCEP data. Moreover, HME has an excellent
432 performance for both intensity and location of the Indian low and the western North Pacific
433 subtropical high. The accurate simulation of the closed-circulation systems in the region can

434 certainly explain the good simulation of 850hPa wind fields. For LME, the western boundary
435 of the western North Pacific subtropical high locates westward to around 110°E, shifted
436 nearly 9 degrees in longitude compared with NCEP (FIG.11c). This situation, that is, under
437 control of the high-pressure system and with too-strong southwest flows, is not favorable to
438 generate precipitation in Southeast China. Hence, LME shows large dry biases in this region.
439 This result is in agreement with our expectation. An accurate simulation of the regional
440 closed-circulation systems, especially the western North Pacific subtropical high, is a
441 guarantee to produce good precipitations in East China.

442 **5 Conclusion**

443 In this paper we revisited the issue about CMIP5 models capability of simulating the
444 regional atmospheric general circulation in East Asia during summer when the summer
445 monsoon plays a dominant role. The particularity of our investigation resides in the
446 utilization of closed-circulation systems, a concept fully relevant and applicable in the region,
447 but insufficiently explored until now in evaluation of climate models. We paid attention on
448 three closed-circulation systems: the South Asian high (SAH), the western North Pacific
449 subtropical high (WNPSH) and the Indian low (IL) at upper, middle and lower troposphere.
450 All models can basically simulate the three closed-circulation systems, although there is a
451 certain inter-model spread and most models underestimate the intensity of the three closed-
452 circulation systems. For the center location, models have the best performance for the South
453 Asian high and the poorest performance for the western North Pacific subtropical high. The
454 latter shows a westward shift by about 6 degrees in longitude in multi-model ensemble
455 average, compared to NCEP reanalysis.

With a set of quantitative measures served as assessment tools, high-skill models which have good comprehensive performance for atmospheric circulation and low-skill models which have the opposite properties are identified respectively. The identification of models capability of simulating the regional atmospheric general circulation has a very pragmatic utility for climate downscaling, since it allows us to select driving models with an adequate consideration for uncertainties in climate simulation. Although the ranking of models depends on the actual measures used for assessment, both groups of high-skill models and low-skill models show consistent behaviors and performances among models for all measures. With our comprehensive and quantitative evaluation, CCSM4, CNRM-CM5, CESM1-CAM5 and NorESM1-M are identified as the high-skill models for simulating the East Asian atmospheric circulation.

The investigation presented here also constituted an occasion for us to check the consistency between models biases in circulation and those in precipitation in East China. This issue is not a trivial question and very few works in the literature investigated it. We analyzed the atmospheric circulation and precipitation in East China from the high-skill models ensemble (HME) and the low-skill models ensemble (LME). This analysis helps us to confirm that biases in the atmospheric circulation impacts biases in precipitations. HME (selected from models performance on atmospheric circulation over East Asia) shows a better simulation of precipitations in East China as well, with 21.3% decrease of dry biases in Southeast China. It was also shown that the physical explanation for this linkage resides in the center position of the western North Pacific subtropical high which determines the quality of 850hPa winds and water vapor transport in Southeast China.

Our quantitative evaluation also reveals some other findings as summarized in the following. CMIP5 models that we examined in this work have generally a suitable capability of simulating the mean state of atmospheric circulation over East Asia. Our five inspected atmospheric fields are well reproduced as a whole. Their Taylor-S indices are larger than 0.84 for 90% of the models. The best performance is for the 500hPa geopotential height with an average Taylor-S index of 0.98. Models skill in simulating the sea level pressure is the lowest, with a Taylor-S index of 0.79. It shows however a significant positive correlation with models resolution. Almost all models underestimate 100hPa geopotential height over East Asia, mainly due to the quite common cold bias in the troposphere.

In terms of methodology, the algorithm that we used to determine indices for closed-circulation systems has the advantage to be applicable for future global warming scenarios. In fact, the critical value dynamically selected as the most outside closed iso-line allows us to deal with models systematic errors in relation to cold biases of the troposphere, as well as to deal with the rising trend of geopotential height in global warming scenarios. He et al. (2018) showed that an 80% fraction of geopotential height rise is attributable to zonal uniform warming through a calculation with the hypsometric equation. Our calculation of closed-circulation-system indices shows very good properties, although an advanced comparison with the algorithm using the concept of eddy geopotential height (He et al., 2018) needs to be done in the future.

Finally, we look forward to applying our diagnostics to new CMIP6 simulations which will be soon available. We believe that what we developed in this paper will provide a

quantitative measure in the assessment of forthcoming CMIP6 simulations, with a meaningful comparison to CMIP5 simulations.

Acknowledgments

We thank two anonymous reviewers and the editor for their constructive comments, which greatly improved the manuscript. We acknowledge the modeling groups, the Program for Climate Model Diagnosis and Intercomparison (PCMDI), the Working Group on Coupled Modelling (WGCM) under World Climate Research Programme, for their roles in making available the WCRP CMIP5 multi-model dataset (https://pcmdi.llnl.gov/). We also appreciate the free access of National Centers for Environmental Prediction – National Center for Atmospheric Research (NCEP/NCAR) datasets (https://www.esrl.noaa.gov/), and the gridded observation precipitation dataset from Dr. Deliang Chen, which can be freely obtained through http://rcg.gvc.gu.se/data/ChinaPrecip/prepdata/ . This work is supported by the National Key Research and Development Program of China (Grant 2017YFA0603804, Grant 2016YFA0600402), the State Key Program of National Natural Science Foundation of China (41230528), Postgraduate Research and Practice Innovation Program of Jiangsu Province (Grant KYLX_0843), the National Science Foundation for Young Scientists of China (Grant 41705055), and the Visiting Fellowship from China Scholarship Council (NO. 201608320196). L. Li acknowledges the support of French ANR (Project China-Trend-Stream) and the National Key Research and Development Program of China (Grant-2018YFC1507704).

References

Akiyama, T. (1975) Southerly transversal moisture flux into the extremely heavy rainfall zone in the Baiu season. Journal of the Meteorological Society of Japan. Ser. II, 53(5), 304-316. https://doi.org/10.2151/jmsj1965.53.5_304

Belleflamme, A., Fettweis, X., Lang, C., and Erpicum, M. (2013) Current and future atmospheric circulation at 500hPa over Greenland simulated by the CMIP3 and CMIP5 global models. Climate Dynamics, 41(7), 2061-2080. https://doi.org/10.1007/s00382-012-1538-2

Chen, D., Ou, T., Gong, L., Xu, C.-Y., Li, W., Ho, C.-H., and Qian, W. (2010) Spatial interpolation of daily precipitation in China: 1951–2005. Advances in Atmospheric Sciences, 27(6), 1221-1232. https://doi.org/10.1007/s00376-010-9151-y

Chen, L., and Frauenfeld, O. W. (2014) A comprehensive evaluation of precipitation simulations over China based on CMIP5 multimodel ensemble projections. Journal of Geophysical Research: Atmospheres, 119(10), 5767-5786. https://doi.org/doi:10.1002/2013JD021190

Chen, W., Jiang, Z., and Li, L. (2011) Probabilistic projections of climate change over China under the SRES A1B scenario using 28 AOGCMs. *Journal of Climate, 24*(17), 4741-4756. https://doi.org/10.1175/2011JCLI4102.1

539 Duan, A., Hu, J., and Xiao, Z. (2013) The Tibetan Plateau summer monsoon in the CMIP5
540 simulations. *Journal of Climate*, *26*(19), 7747-7766. https://doi.org/10.1175/JCLI-D-12-
541 00685.1

542 Gamble, D.W., Parnell, D.B. and Curtis, S. (2008) Spatial variability of the Caribbean mid-
543 summer drought and relation to north Atlantic high circulation. International Journal of
544 Climatology, 28(3), pp.343-350. https://doi.org/10.1002/joc.1600

545 Gleckler, P. J., Taylor, K. E., and Doutriaux, C. (2008) Performance metrics for climate
546 models. *Journal of Geophysical Research: Atmospheres*, *113*(D6).

547 https://doi.org/10.1029/2007JD008972

548 Gong, H., Wang, L., Chen, W., Wu, R., Wei, K., and Cui, X. (2014) The climatology and
549 interannual variability of the East Asian winter monsoon in CMIP5 models. *Journal of*
550 *Climate*, *27*(4), 1659-1678. https://doi.org/10.1175/JCLI-D-13-00039.1

551 Hameed, S., and Reimer, N. (2012) Relationship of Sahel Precipitation and Atmospheric
552 Centers of Action. *Advances in Meteorol*ogy, 2012, 1-8.
553 https://doi.org/10.1155/2012/953853

554 Han, J.-P., and Wang, H.-J. (2007) Features of interdecadal changes of the East Asian
555 summer monsoon and similarity and discrepancy in ERA-40 and NCEP/NCAR reanalysis.
556 *Chinese Journal of Geophysics*, *50*(6), 1666-1676. (In Chinese)

557 He, B., and Wen-Ting, H. (2015) Assessment of the summer South Asian high in eighteen
558 CMIP5 models. *Atmospheric and Oceanic Science Letters*, *8*(1), 33-38.

559 http://dx.doi.org/10.3878/AOSL20140069

He, C., and Zhou, T. (2014) The two interannual variability modes of the Western North Pacific Subtropical High simulated by 28 CMIP5–AMIP models. *Climate Dynamics, 43*(9-10), 2455-2469. https://doi.org/10.1007/s00382-014-2068-x

Huang, D.-Q., Zhu, J., Zhang, Y.-C., and Huang, A.-N. (2013) Uncertainties on the simulated summer precipitation over Eastern China from the CMIP5 models. *Journal of Geophysical Research: Atmospheres*, 118(16), 9035–9047. https://doi.org/10.1002/jgrd.50695

Huang, Y., and Li, X. (2015a) The interdecadal variation of the western Pacific subtropical high as measured by 500hPa eddy geopotential height. *Atmospheric and Oceanic Science Letters*, 8(6):371–375. https://doi.org/10.3878/AOSL20150038

Huang, Y., Wang, H., Fan, K., and Gao, Y. (2015b) The western Pacific subtropical high after the 1970s: westward or eastward shift? *Climate Dynamics*, 44(7–8):2035–2047. https://doi.org/10.1007/s00382-014-2194-5

Jiang, D., and Tian, Z. (2013) East Asian monsoon change for the 21st century: Results of CMIP3 and CMIP5 models. *Chinese Science Bulletin, 58*(12), 1427-1435. https://doi.org/10.1007/s11434-012-5533-0

Jiang, D., Tian, Z., and Lang, X. (2016) Reliability of climate models for China through the IPCC Third to Fifth Assessment Reports. *International Journal of Climatology, 36*(3), 1114-1133. https://doi.org/10.1002/joc.4406

Jiang, Z., Li, W., Xu, J., and Li, L. (2015) Extreme precipitation indices over China in CMIP5 models. Part I: Model evaluation. *Journal of Climate, 28*(21), 8603-8619. https://doi.org/10.1175/JCLI-D-15-0099.1

581 Jiang, Z., Song, J., Li, L., Chen, W., Wang, Z., and Wang, J. (2012) Extreme climate events
582 in China: IPCC-AR4 model evaluation and projection. *Climatic Change*, *110*(1-2), 385-401.
583 https://doi.org/10.1007/s10584-011-0090-0

584 Khon, V. C., and Mokhov, I. (2006) Model estimates for the sensitivity of atmospheric
585 centers of action to global climate changes. *Izvestiya, Atmospheric and Oceanic Physics*,
586 *42*(6), 688-695. https://doi.org/10.1134/S0001433806060028

587 Kitoh, A., Kusunoki, S. (2008) East Asian summer monsoon simulation by a 20-km mesh
588 AGCM. *Climate Dynamics*, 31 (4): 389-401. https://doi.org/10.1007/s00382-007-0285-2

589 Kusunoki, S., Yoshimura, J., Yoshimura, H., Noda, A., Oouchi, K., and Mizuta, R. (2006)
590 Change of Baiu rain band in global warming projection by an atmospheric general circulation
591 model with a 20-km grid size. *Journal of the Meteorological Society of Japan. Ser. II*, 84 (4):
592 581-611. https://doi.org/10.2151/jmsj.84.581

593 Li, D., Zou, L., Zhou T. (2018) Regional air-sea coupled model simulation for two types of
594 extreme heat in North China. *Climate Dynamics*, 50: 2107-2120.
595 https://doi.org/10.1007/s00382-017-3738-2

596 Li, J., Yu, R., Yuan, W., Chen, H., Sun, W. and Zhang, Y. (2015) Precipitation over East
597 Asia simulated by NCAR CAM5 at different horizontal resolutions. *Journal of Advances in*
598 *Modeling Earth Systems*, *7*(2), pp.774-790. https://doi.org/10.1002/2014MS000414

599 Li, W., Li, L., Fu, R., Deng, Y. and Wang, H. (2011) Changes to the North Atlantic
600 subtropical high and its role in the intensification of summer rainfall variability in the

601 southeastern United States. *Journal of Climate*, *24*(5), pp.1499-1506.
602 https://doi.org/10.1175/2010JCLI3829.1

603 Lin, A.L., Li, C.H., Gu, D.J. and Zheng, B. (2012) Variation and causes of persistent drought
604 events in Guangdong Province. *Journal of Tropical Meteorology*, 18(1), p.54.
605 https://doi.org/10.3969/j.issn.1006-8775.2012.01.006

606 Liu Y. and Ding Y. (2008) Analysis and numerical simulation of the teleconnection between
607 Indian summer monsoon and precipitation in North China. *Acta Meteorologica Sinica*, 66(5),
608 789-799.

609 Liu, Y., Li, W., Zuo, J., and Hu, Z. (2014) Simulation and projection of the western pacific
610 subtropical high in CMIP5 models. *Journal of Meteorological Research, 28*(3), 327-340.
611 https://doi.org/10.1007/s13351-014-3151-2

612 Matsumura, S., Sugimoto, S. and Sato, T. (2015) Recent intensification of the western Pacific
613 subtropical high associated with the East Asian summer monsoon. *Journal of Climate*, *28*(7),
614 pp.2873-2883. https://doi.org/10.1175/jcli-d-14-00569.1

615 Meehl, G. A., Arblaster, J. M., and Tebaldi, C. (2005) Understanding future patterns of
616 increased precipitation intensity in climate model simulations. *Geophysical Research Letters*,
617 *32*(18). https://doi.org/10.1029/2005GL023680

618 Ou, T., Chen, D., Linderholm, H. W., and Jeong, J.-H. (2013) Evaluation of global climate
619 models in simulating extreme precipitation in China. *Tellus A: Dynamic Meteorology and*
620 *Oceanography*, *65*(1), 19799. https://doi.org/10.3402/tellusa.v65i0.19799

621 Preethi, B., Mujumdar, M., Prabhu, A., and Kripalani, R. (2017) Variability and
622 teleconnections of South and East Asian summer monsoons in present and future projections

of CMIP5 climate models. *Asia-Pacific Journal of Atmospheric Sciences, 53*(2), 305-325. https://doi.org/10.1007/s13143-017-0034-3

Qu, X., Huang, G. (2014) The decadal variability of the tropical Indian Ocean SST- the South Asian High relation: CMIP5 model study. *Climate Dynamics*. https://doi.org/10.1007/S00382-014-2285-3

Radić, V., and Clarke, G. K. (2011) Evaluation of IPCC models' performance in simulating late-twentieth-century climatologies and weather patterns over North America. *Journal of Climate, 24*(20), 5257-5274. https://doi.org/10.1175/JCLI-D-11-00011.1

Ren, L., Wang, P., Li. L., and Guo, D. (2011) Analysis on characteristics of India Low anomaly and its relationship with precipitation in India and China in the same period. *J. Trop. Meteor.* 27(4), 509-581. (In Chinese) https://doi.org/10.3969/j.issn.1004-4965.2011.04.008

Rossby, C. G. (1939) Relation between variations in the intensity of the zonal circulation of the atmosphere and the displacements of the semi-permanent centers of action. J. Mar. Res., 2, 38-55.

Seo, K.-H., Ok, J., Son, J.-H., and Cha, D.-H. (2013) Assessing future changes in the East Asian summer monsoon using CMIP5 coupled models. *Journal of Climate, 26*(19), 7662-7675. https://doi.org/10.1175/JCLI-D-12-00694.1

Sheffield, J., Barrett, A.P., Colle, B., Nelun Fernando, D., Fu, R., Geil, K.L., Hu, Q., Kinter, J., Kumar, S., Langenbrunner, B. and Lombardo, K. (2013) North American climate in CMIP5 experiments. Part I: Evaluation of historical simulations of continental and regional

643 climatology. Journal of Climate, 26(23), pp.9209-9245. https://doi.org/10.1175/jcli-d12-
644 00593.1

645 Sheffield, J., Camargo, S.J., Fu, R., Hu, Q., Jiang, X., Johnson, N., Karnauskas, K.B., Kim,
646 S.T., Kinter, J., Kumar, S. and Langenbrunner, B. (2013) North American climate in CMIP5
647 experiments. Part II: Evaluation of historical simulations of intraseasonal to decadal
648 variability. Journal of Climate, 26(23), pp.9247-9290. https://doi.org/10.1175/jcli-d-12-
649 00592.1

650 Simmonds, I., Bi, D., and Hope, P. (1999) Atmospheric water vapor flux and its association
651 with rainfall over china in summer. *Journal of Climate, 12*(5), 1353-1367.

652 https://doi.org/10.1175/1520-0442(1999)012<1353:AWVFAI>2.0.CO;2

653 Song, F. and Zhou, T. (2014) Interannual variability of East Asian summer monsoon
654 simulated by CMIP3 and CMIP5 AGCMs: Skill dependence on Indian Ocean–western
655 Pacific anticyclone teleconnection. Journal of Climate, 27(4), pp.1679-1697.
656 https://doi.org/10.1175/jcli-d-13-00248.1

657 Song, F. and Zhou, T. (2014) The climatology and interannual variability of East Asian
658 summer monsoon in CMIP5 coupled models: Does air–sea coupling improve the simulations?
659 Journal of Climate, 27(23), pp.8761-8777. https://doi.org/10.1175/jcli-d-14-00396.1

660 Sperber, K., Annamalai, H., Kang, I.-S., Kitoh, A., Moise, A., Turner, A., Wang, B., Zhou,
661 T. (2013) The Asian summer monsoon: an intercomparison of CMIP5 vs. CMIP3 simulations
662 of the late 20th century. *Climate Dynamics, 41*(9-10), 2711-2744.

663 https://doi.org/10.1007/s00382-012-1607-6

664 Su, F., Duan, X., Chen, D., Hao, Z. and Cuo, L. (2013) Evaluation of the global climate
665 models in the CMIP5 over the Tibetan Plateau. *Journal of Climate*, *26*(10), pp.3187-3208.
666 https://doi.org/10.1175/jcli-d-12-00321.1
667 Su, T., Xue, F. and Zhang, H. (2014) Simulating the intraseasonal variation of the East Asian
668 summer monsoon by IAP AGCM4. 0. *Advances in Atmospheric Sciences*, *31*(3), pp.570-580.
669 https://doi.org/10.1007/s00376-013-3029-8
670 Sun, X., Wang, P., and Wang, J. (2017) An assessment of the atmospheric centers of action
671 in the northern hemisphere winter. *Climate Dynamics*, *48*(3-4), 1031-1047.
672 https://doi.org/10.1007/s00382-016-3126-3
673 Sun, X., Wang, P., Wang, X., and Zhi, H (2013) A calculation scheme of the area and
674 intensity indices on North Pacific subtropical high in winter. *Transactions of Atmospheric*
675 *Sciences*. 36(5), 586-592. (In Chinese) https://doi.org/10.13878/j.cnki.dqkxxb.2013.05.004
676 Taylor, K. E. (2001) Summarizing multiple aspects of model performance in a single diagram.
677 *Journal of Geophysical Research: Atmospheres*, *106*(D7), 7183-7192.
678 https://doi.org/10.1029/2000JD900719
679 Tian, L., Jiang, Z., and Chen, W. (2016) Evaluation of summer average circulation simulation
680 over East Asia by CMIP5 climate models. *Climatic and Environmental Research*. 21(4), 380-
681 392. (In Chinese) https://doi.org/10.3878/j.issn.1006-9585.2016.13089
682 Wang, P., Lu, C., Guan, Z., Li, S., Yao, S., and Yan, L. (2007) Definition and calculation
683 of three circulation indices for closed pressure systems. *Journal of Nanjing Institute of*

Meteorology. 30(6), 730-735. (In Chinese)
https://doi.org/10.13878/j.cnki.dqkxxb.2007.06.001

Wang, P., Wang, J. X., Zhi, H., Wang, Y., and Sun, X. (2012) Circulation indices of the Aleutian low pressure system: Definitions and relationships to climate anomalies in the northern hemisphere. *Advances in Atmospheric Sciences*, *29*(5), 1111-1118. https://doi.org/10.1007/s00376-012-1196-7

Wang, P., Zhao, H., Ren, L., Luo, X., and Guo, D. (2010) Calculation method of center position index for closed pressure systems. *Transactions of Atmospheric Sciences.* 33(5), 520-526. (In Chinese) https://doi.org/10.13878/j.cnki.dqkxxb.2010.05.001

Wang, Y., and Zhou, L. (2005) Observed trends in extreme precipitation events in China during 1961–2001 and the associated changes in large-scale circulation. *Geophysical Research Letters*, *32*(9). https://doi.org/10.1029/2005GL022574

Wei, K., Xu, T., Du, Z., Gong, H., and Xie, B. (2014) How well do the current state-of-the-art CMIP5 models characterise the climatology of the East Asian winter monsoon? *Climate Dynamics*, *43*(5-6), 1241-1255. https://doi.org/10.1007/s00382-013-1929-z

Wu, L. and Wang, C. (2015) Has the western Pacific subtropical high extended westward since the late 1970s? *Journal of Climate*, *28*(13), 5406-5413.
https://doi.org/10.1175/jcli-d-14-00618.1

Xu, J., Gao, Y., Chen, D., Xiao, L., and Ou, T. (2017) Evaluation of global climate models for downscaling applications centred over the Tibetan Plateau. *International Journal of Climatology*, *37*(2), 657-671. https://doi.org/10.1002/joc.4731.

705 Xu, X. D., Shi, X. Y., Wang, Y. Q., Peng, S. Q., and Shi, X. H. (2008) Data analysis and
706 numerical simulation of moisture source and transport associated with summer precipitation
707 in the Yangtze River Valley over China. *Meteorology and Atmospheric Physics, 100*(1-4),
708 217-231. https://doi.org/10.1007/s00703-008-0305-8

709 Xue, X., Chen, W., and Chen, S. (2016) The climatology and interannual variability of the
710 South Asia high and its relationship with ENSO in CMIP5 models. Climate Dynamics,
711 48(11-12), 3507–3528. https://doi.org/10.1007/s00382-016-3281-6

712 Yao, J., Zhou, T., Guo, Z., Chen, X., Zou, L. and Sun, Y. (2017) Improved performance of
713 high-resolution atmospheric models in simulating the East Asian summer monsoon rain belt.
714 *Journal of Climate, 30*(21), pp.8825-8840. https://doi.org/10.1175/JCLI-D-16-0372.1

715 You, Q., Jiang, Z., Wang, D., Pepin, N., and Kang, S. (2018) Simulation of temperature
716 extremes in the Tibetan Plateau from CMIP5 models and comparison with gridded
717 observations. *Climate Dynamics, 51*(1), 355-369. https://doi.org/10.1007/s00382-017-3928-
718 y

719 You, Q., Kang, S., Aguilar, E., Pepin, N., Flügel, W.-A., Yan, Y., Xu, Y., Zhang Y., Huang,
720 J. (2011) Changes in daily climate extremes in China and their connection to the large scale
721 atmospheric circulation during 1961–2003. *Climate Dynamics, 36*(11-12), 2399-2417.
722 https://doi.org/10.1007/s00382-009-0735-0

723 Zeng, G., Wang, W.-C., and Shen, C. (2012) Association of the Rainy Season Precipitation
724 with Low-Level Meridional Wind in the Yangtze River Valley and North China. *Journal of*
725 *Climate, 25*(2), 792-799. https://doi.org/10.1175/jcli-d-10-05027.1

726 Zhang, R. (2001) Relation of water vapor transport from Indian monsoon with that over East
727 Asia and summer rainfall in China. *Advances in Atmospheric Sciences,* 18, 1005-1007.

728 Zhou, T. J., and Yu, R. C. (2005) Atmospheric water vapor transport associated with typical
729 anomalous summer rainfall patterns in China. *Journal of Geophysical Research:*
730 *Atmospheres, 110*(D8). https://doi.org/10.1029/2004JD005413

731 Zhou, T., Wang, B., Yu, Y., Liu, Y., Zheng, W., Li, L., Wu, B., Lin, P., Guo, Z., Man, W.
732 and Bao, Q. (2018a) The FGOALS climate system model as a modeling tool for supporting
733 climate sciences: An overview. Earth and Planetary Physics, 2(4), pp.276-291.
734 https://doi.org/10.26464/epp2018026

735 Zhou, T., Wu, B., Guo, Z., He, C., Zou, L., et al. (2018b) A review of East Asian summer
736 monsoon simulation and projection: Achievements and problems, opportunities and
737 challenges. *Chinese Journal of Atmospheric Sciences*, 42 (4): 902−934. (In Chinese)
738 https://doi.org/10.3878/j.issn.1006-9895.1802.17306

739

740